DOI: https://doi.org/10.15625/0868-3166/22638

Electron-phonon coupling effects on the van Hove singularity in topological crystalline insulators

Doan Quoc Khoa¹, Nguyen Tien Dung², Tran Tien³, and Bui Dinh Hoi^{4,†}

E-mail: †buidinhhoi@hueuni.edu.vn

Received 1 April 2025; Accepted for publication 14 May 2025; Published 29 May 2025

Abstract. In this study, we examine the influence of electron-phonon coupling (EPC) on the van Hove singularities on the SnTe(001) surface as a topological crystalline insulator (TCI). To do this, we calculate the electronic density of states (DOS) and investigate its changes according to the parameters characteristic of the EPC. The effect of EPC is incorporated in the modified momentum (wave number) components along the x- and y-directions. The results show that when varying the EPC strength along the x-direction (λ_x) , the number and position of the van Hove singularities remain unchanged, but their height decreases significantly. As λ_x is sufficiently large, these singularities vanish, and an energy gap emerges. In contrast, when the EPC strength λ_v is altered within a range similar to λ_x , the change in DOS is nearly negligible, and a significant EPC is required to observe any small changes. The difference in the DOS changes with respect to EPC strength between the x- and y-directions highlights the anisotropy of the SnTe(001) surface. Furthermore, the influence of the intervalley scattering parameters, n and δ , on the electronic properties of the system is also examined. The results show that these parameters significantly affect the density of states (DOS), both in the absence and presence of EPC. Overall, our findings demonstrate that the electronic characteristics of the SnTe(001) surface can be effectively tuned through EPC – by altering factors that influence lattice vibrations, such as temperature or substrate material - as well as through changes in intervalley scattering, which is governed by the surface roughness of the TCI.

Keywords: Topological insulator; electronic structure; density of states; van Hove singularity; phonon.

Classification numbers: 71.20.-b; 73.22.-f; 71.10.-w; 71.38.-k; 73.20.-r.

¹The University of Danang - University of Science and Technology, Da Nang 550000, Vietnam

²School of Engineering and Technology, Vinh University, 182 Le Duan street, Vinh City, Nghe An province, Vietnam

³University of Medicine and Pharmacy, Hue University, Hue 530000, Vietnam

⁴Faculty of Physics, University of Education, Hue University, Hue 530000, Vietnam

1. Introduction

Topological materials have attracted significant interest in the field of condensed matter physics due to their unique physical properties [1,2]. The topological crystalline insulator (TCI) was first theoretically proposed by Liang Fu in 2011 [3], where topological states are protected by crystal symmetry (mirror symmetry) [3–9], in addition to the time-reversal symmetry in previously discovered topological insulators [10–13]. Unlike strong topological insulators, TCIs feature an even number of Dirac states, arising from their inherent C_2 and C_4 rotational symmetries. The abundance of gapless Dirac cones in TCIs offers significant potential for applications in spintronics and valleytronics. One of the first theoretical and experimental predictions for TCIs was IV-VI semiconductors with a rocksalt structure, with SnTe being a typical representative [5–8]. Therefore, TCIs of this type are also classified as SnTe-class TCIs. In addition to the SnTe-class TCIs mentioned above, there are other TCIs that have been theoretically predicted [14–16].

A van Hove singularity (vHS) occurs at points in the dispersion relation (the relation between energy/frequency and momentum) where there is a saddle point, maximum, or minimum, causing the gradient of the energy dispersion to be zero at these points [17, 18]. This concept was initially introduced by Léon van Hove in his study of phonon densities of states, which describes the frequency distribution of elastic lattice vibrations in a crystal [19]. In electronic band structures, a vHS leads to a peak or divergence in the electronic density of states (DOS), indicating a high density of electronic states at specific energies. The presence of a vHS enhances electronic interactions, which can influence phenomena such as superconductivity, magnetism, and density wave instabilities [17, 20–22]. These effects also lead to strong optical absorption features and anomalies in thermodynamic properties, making the understanding and tuning of vHS crucial for predicting electronic, optical, and thermodynamic behavior in materials [22–26].

There are numerous methods available to tune the electronic properties of a material, including doping to modify the concentration or type of charge carriers, surface adsorption, application of strain, formation of heterojunctions, temperature variation, exposure to external electromagnetic fields, proximity effects, and electron–phonon interaction, among others [27–33]. Among these, electron–phonon interaction is particularly significant, as it modifies not only the electronic energy dispersion but also the phonon spectrum. To date, the effects of electron-phonon coupling (EPC) on the vHS in TCIs have remained largely unexplored – a gap this study aims to fill. We examine how lattice vibrations, through EPC, break spatial symmetry and lead to direction-dependent renormalization of the Fermi velocity. This anisotropy in low-energy electron dispersion alters the electronic DOS, thereby modulating the vHS. Incorporating EPC is crucial for accurately predicting and understanding the electronic and thermal properties of materials. Our results reveal substantial deviations in the electronic DOS of EPC-modified TCI lattices compared to their pristine counterparts.

The paper is organized as follows. In Sec. 2, we provide an overview of the Hamiltonian model and the DOS for both pristine and EPC-induced Dirac cones on the (001) surface of SnTe. In Sec. 3, we present numerical results, which explore various scenarios regarding the strength of EPC. Finally, Sec. 4 offers a summary of our study.

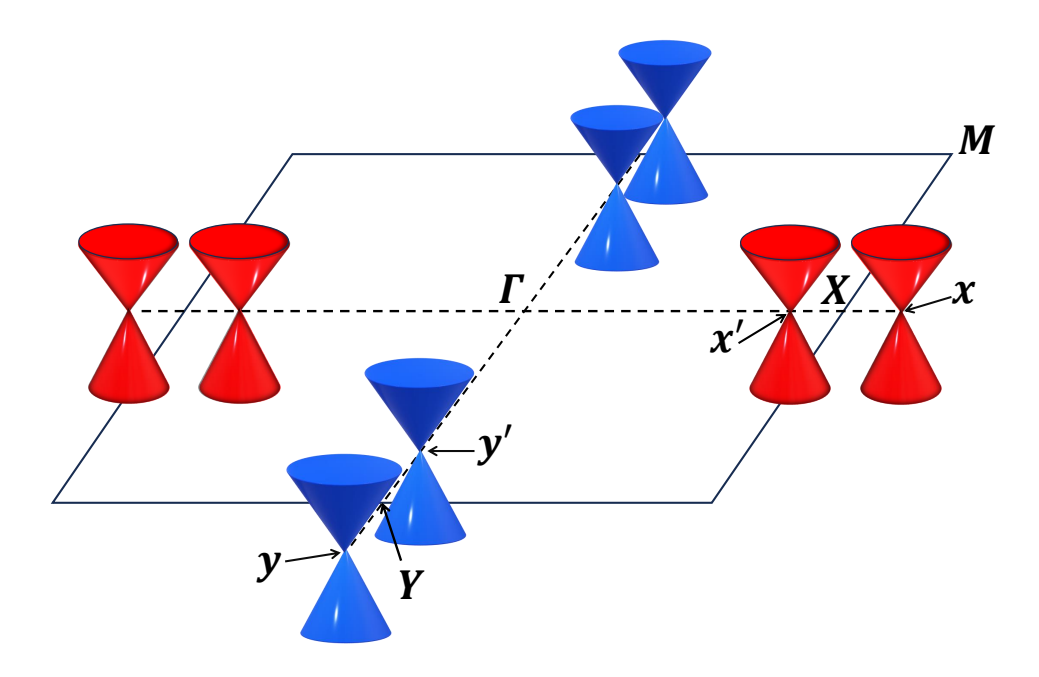


Fig. 1. A sketch of the coaxial energy dispersion cones (Dirac cones) in the low-energy limit, occurring around the X and Y points of the projected surface Brillouin zone for the pristine SnTe(001) topological insulating surface. The Dirac points are located at $x(x') = \pm \sqrt{n^2 + \delta^2}/\eta_1$ and $y(y') = \mp \sqrt{n^2 + \delta^2}/\eta_2$. The gapless states are protected by the crystalline C_2 and C_4 rotational symmetries.

2. Low-energy Hamiltonian and density of states of SnTe(001) surface

We begin with a well-established continuum model [5–8, 34, 35] that describes the Dirac fermions on the SnTe(001) surface. In this model, the effective electronic bands are formed by the p orbitals of the Sn and Te sublattices, with the ground states being a mix of spin-orbitally coupled states. This model preserves the fundamental physics of TCIs and separates the coupled coaxial Dirac cones at low energies (see Fig. 1 for details). Specifically, two cones position along the X- Γ -X direction of the projected surface Brillouin zone (SBZ) at points x and x', while two other cones are along the Y- Γ -Y direction at points y and y'. The Hamiltonian at the X point, in the absence of any perturbations (i.e., the pristine case), is given by (we set $\hbar = 1$) [30, 34–37]

$$H_X^{\text{pristine}} = \eta_1 k_x \hat{\sigma}_y - \eta_2 k_y \hat{\sigma}_x + n \hat{\tau}_x + \delta \hat{\sigma}_y \hat{\tau}_y, \tag{1}$$

where k_x (k_y) is the carrier momentum along the x (y) direction; $\eta_1 = 1.3$ eV.Å and $\eta_2 = 2.4$ eV.Å are the Fermi velocities along the x and y directions, respectively [5, 34, 38]. $\hat{\sigma} = (\hat{\sigma}_x, \hat{\sigma}_y)$ denotes the Pauli matrices for the two spin components (i.e., the Kramers doublet), while the Pauli matrices representing the cation–anion degree of freedom are given by $\hat{\tau} = (\hat{\tau}_x, \hat{\tau}_y)$. The parameters n and δ are referred to as intervalley scattering parameters in momentum space [36, 38], which are primarily affected by the surface roughness of the TCI surface. Therefore, proximity effects or

changes in the atomic configuration at the surface can modify these values. The influence of these two parameters will be analyzed in detail at the end of Sec. 3. In addition, it should be noted that utilizing the C_4 rotational symmetry, the corresponding Hamiltonians for the Y point can be easily derived [39].

Regarding the effect of EPC, it is important to emphasize that our theoretical framework relies on the modulation of orbital degrees of freedom, arising from the interaction between substrate atoms and the host Sn and Te sublattices—both of which vibrate around their equilibrium positions. This interaction has a significant impact on the electronic properties of the system [40]. In solids, electrons can interact with these lattice vibrations, resulting in changes to both their momentum and energy. In our model, considering the orbital characteristics of the bands, the electronic momentum space is shifted according to the EPC strength, which arises from lattice displacements, generated through thermal effects, for example [41–43]. This shift first breaks the spatial symmetry, and then, the Fermi velocities of the electronic bands are normalized along the direction of symmetry breaking. The incorporation of this effect into momentum space introduces an EPC-induced gauge field vector potential $\vec{A} = (\frac{\lambda_x}{v_x}, -\frac{\lambda_y}{v_y})$, where λ_x (λ_y) denotes the EPC strength along the x (y) axis. As a result, in the linear order of the EPC strength, one can define the modulated momenta as

$$\tilde{k}_x = k_x + \frac{\lambda_x}{v_x} \,, \tag{2a}$$

$$\tilde{k}_{y} = k_{y} - \frac{\lambda_{y}}{\nu_{y}}.$$
 (2b)

Therefore, the Hamiltonian at the X point, when accounting for EPC, is succinctly written as [30,34-37].

$$H_X^{\text{EPC}} = \eta_1 \tilde{k}_x \hat{\sigma}_y - \eta_2 \tilde{k}_y \hat{\sigma}_x + n \hat{\tau}_x + \delta \hat{\sigma}_y \hat{\tau}_y. \tag{3}$$

Now let us introduce the expression for the electronic DOS, a quantity from which we will extract the necessary information about the vHS. As well-known, the electronic DOS is described in terms of the imaginary parts of the diagonal Green's functions via [30,44]

$$D(\mathscr{E}) = -\frac{1}{\pi} \sum_{\beta=1}^{4} \sum_{\vec{k} \in SBZ} Im \left[G_{\beta\beta}(\vec{k}, \mathscr{E}) \right], \tag{4}$$

where β refers to both spin and surface degrees of freedom. Generically, the Green's function matrix is calculated using the relation $G(\vec{k},\mathscr{E}) = \left[\mathscr{E} + \mathrm{i}\,\eta - \mathscr{H}(\vec{k})\right]^{-1}$ where $\mathscr{H}(\vec{k})$ is the matrix representation of the Hamiltonians in Eq. (1) and Eq. (3) for the pristine and EPC-included case, respectively, \mathscr{E} is the energy bandwidth and $\eta = 0.1$ meV is a small real number (phenomenological factor).

3. Numerical results

In this section, we will clarify the influence of EPC on the vHS by performing numerical calculations to obtain the DOS. First, we plot the three-dimensional energy dispersion for the pristine case (without EPC) in the low-energy limit, obtained by diagonalizing the Hamiltonian in Eq. (1) when n = 0.07 eV and $\delta = 0.026$ eV [34, 36], as shown in Fig. 2. It can be seen that

Dirac cones appear at certain special positions. At the wave vector $\vec{k}=(0,0)$, we have two Diraclike cones located at energy values $\mathcal{E}=\pm\sqrt{n^2+\delta^2}$, while the two Dirac cones near the X point, shown in Fig. 1, have zero energy with coordinates $x=\sqrt{n^2+\delta^2}/\eta_1$ and $x'=-\sqrt{n^2+\delta^2}/\eta_1$. Notably, there are saddle points S and S' with coordinates $S=(0,+n/\eta_2)$ and $S'=(0,-n/\eta_2)$. These points are responsible for generating the vHS near the Fermi surface.

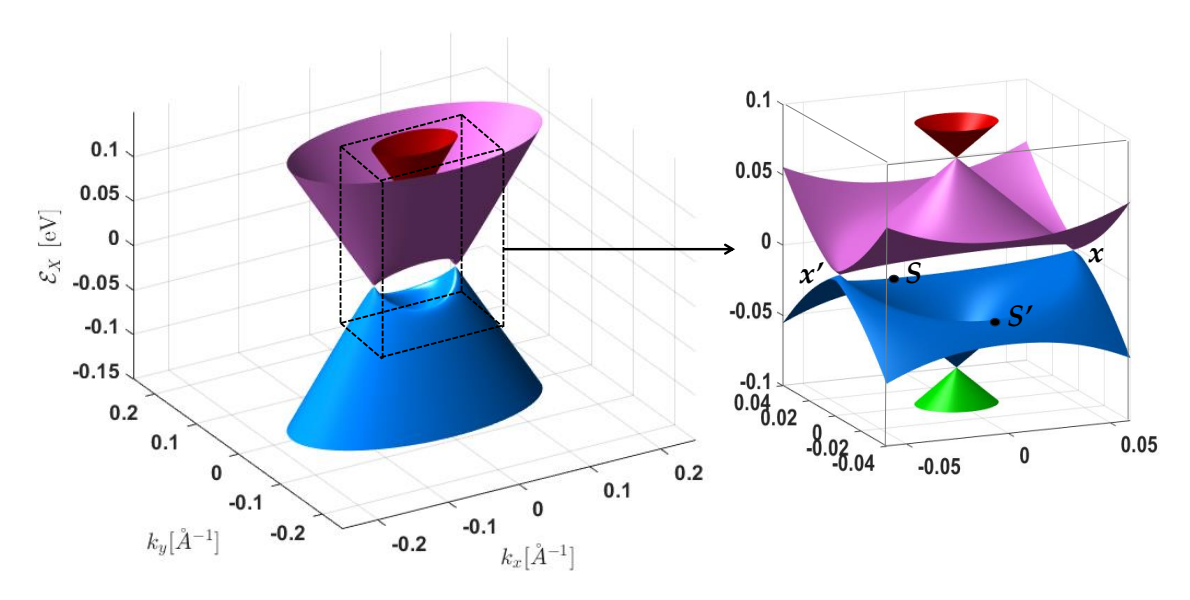


Fig. 2. Three-dimensional energy dispersion of Dirac fermions on the SnTe(001) surface near the *X* point of the SBZ obtained from the Hamiltonian in Eq. (1). Two saddle points contribute to the carrier dynamics with the coordinates $S = (0, +n/\eta_2)$ and $S' = (0, -n/\eta_2)$. Also, the Dirac-like cones at $\vec{k} = (0,0)$ are located at energies $\mathcal{E} = \pm \sqrt{n^2 + \delta^2}$, while two Dirac cones at $\mathcal{E} = 0$ have the coordinates $x = \sqrt{n^2 + \delta^2}/\eta_1$ and $x' = -\sqrt{n^2 + \delta^2}/\eta_1$. Here, n = 0.07 eV and $\delta = 0.026$ eV as taken from Refs. [34, 36].

Now, we will focus on the core of this study, which is to examine the influence of EPC on the vHS in the electronic DOS of the SnTe(001) surface. To clearly see the directional difference of EPC, we will investigate the change in the DOS by separately varying λ_x and λ_y . In Fig. 3, we plot the DOS as a function of electronic energy in the range from -0.15 eV to +0.15 eV with $-0.25 \le k_x \le 0.25$ and $-0.25 \le k_y \le 0.25$ at four different values of λ_x when $\lambda_y = 0$. Along the black curve, which corresponds to the case without EPC, we can observe the appearance of two singularities that are symmetric around the zero energy value. These correspond to the saddle points in the valence and conduction bands, as shown in Fig. 2. It can be seen that as λ_x increases, the intensity of the singularities decreases significantly; however, they remain at their initial energy values and the system still maintains a semi-metallic phase, as indicated by the red, blue, and green curves in Fig. 3. Notably, when $\lambda_x = 0.45$ eV, the van Hove singularities completely disappear, and a band gap of about 0.1 eV opens up. This indicates a semimetal-to-semiconductor phase transition. To better understand the relationship between the DOS and the electronic energy band

structure when λ_x is changed, we plot the three-dimensional energy dispersion in the wavevector domain and the values of λ_x as shown in Fig. 4. It can be seen that when λ_y is zero and λ_x is changed, the energy dispersion spectrum shifts significantly in the x-direction towards higher momentum, and the energy values at the saddle points remain unchanged. Some electronic states gradually disappear within the wavevector range considered, and when $\lambda_x = 0.45$ eV, the energy bands in the conduction band and the valence band completely separate, creating a band gap as shown in Fig. 3. Similarly, we continue to examine the effect of EPC in the y-direction. In Figs. 5 and 6, we plot the DOS and energy dispersion, respectively, when λ_x is fixed at 0 and λ_y is varied from 0.15 eV to 0.45 eV within the energy and wavevector ranges as shown in Figs. 3 and 4. It can be seen in Fig. 5 that when λ_v is varied, the DOS changes insignificantly, and the van Hove singularities are almost unaffected by the EPC in the y-direction. This characteristic is illustrated by the very slow shift of the energy dispersion in the y-direction towards larger momentum, and the dispersion shape remains unchanged as λ_v increases. In short, the difference in the change of DOS between the x- and y-directions under the influence of EPC reflects the anisotropic nature of the SnTe(001) surface. Also, it is worth noting that due to translational symmetry, the DOS remains unchanged if we replace λ_i by $-\lambda_i$ (i = x or y) in the Hamiltonian (3), whereas the energy dispersion (the Dirac cones) will be shifted in the opposite way.

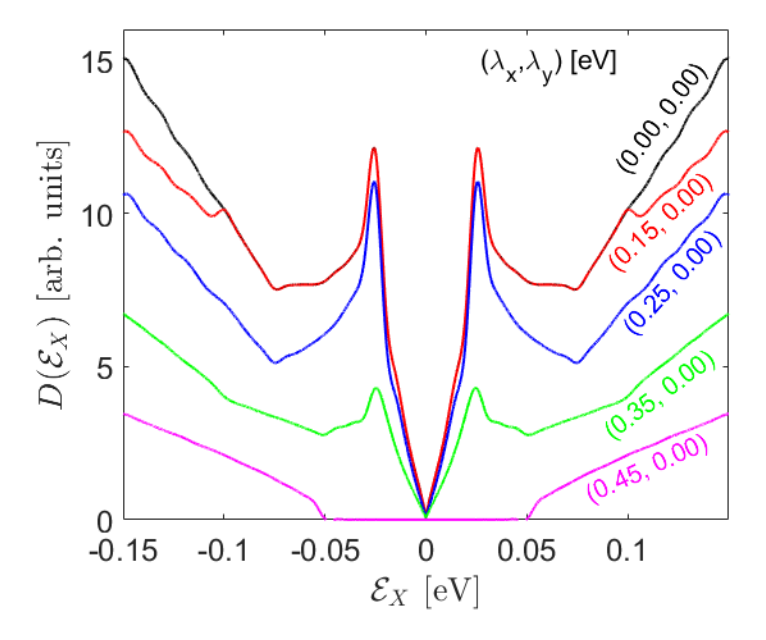


Fig. 3. The variation of the electronic DOS on the SnTe(001) surface near the X point of SBZ as a function of the EPC strength λ_x , with $\lambda_y = 0$. The van Hove singularities gradually decrease in intensity with increasing λ_x and disappear when λ_x becomes sufficiently large, also the system shows a phase transition from a semimetal to a conventional semiconductor. Here, n = 0.07 eV and $\delta = 0.026$ eV.

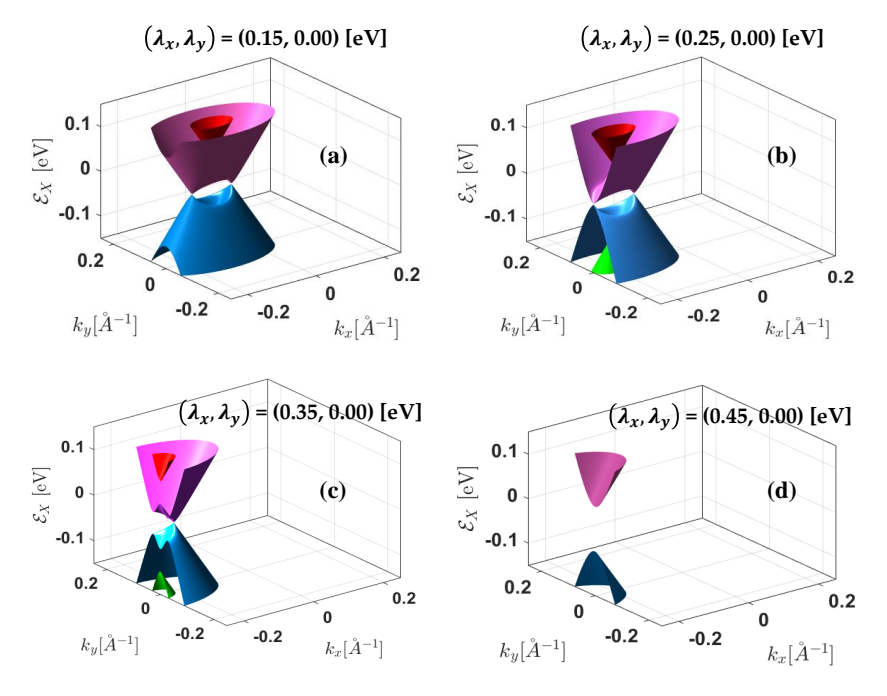


Fig. 4. The evolution of the three-dimensional energy band structure of Dirac fermions on the SnTe(001) surface near the X point, as the EPC strength along the x-direction is varied, shows a significant shift of the bands along the same direction. Here, n = 0.07 eV and $\delta = 0.026$ eV.

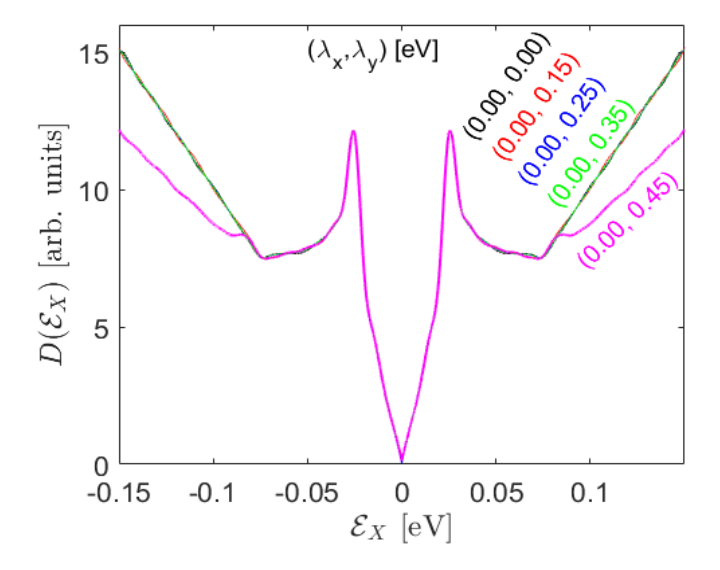


Fig. 5. The electronic DOS of the SnTe(001) surface near the *X* point of SBZ for different values of EPC strength λ_y and $\lambda_x = 0$. The van Hove singularities are almost unaffected by the EPC in the *y*-direction. Here, n = 0.07 eV and $\delta = 0.026$ eV.

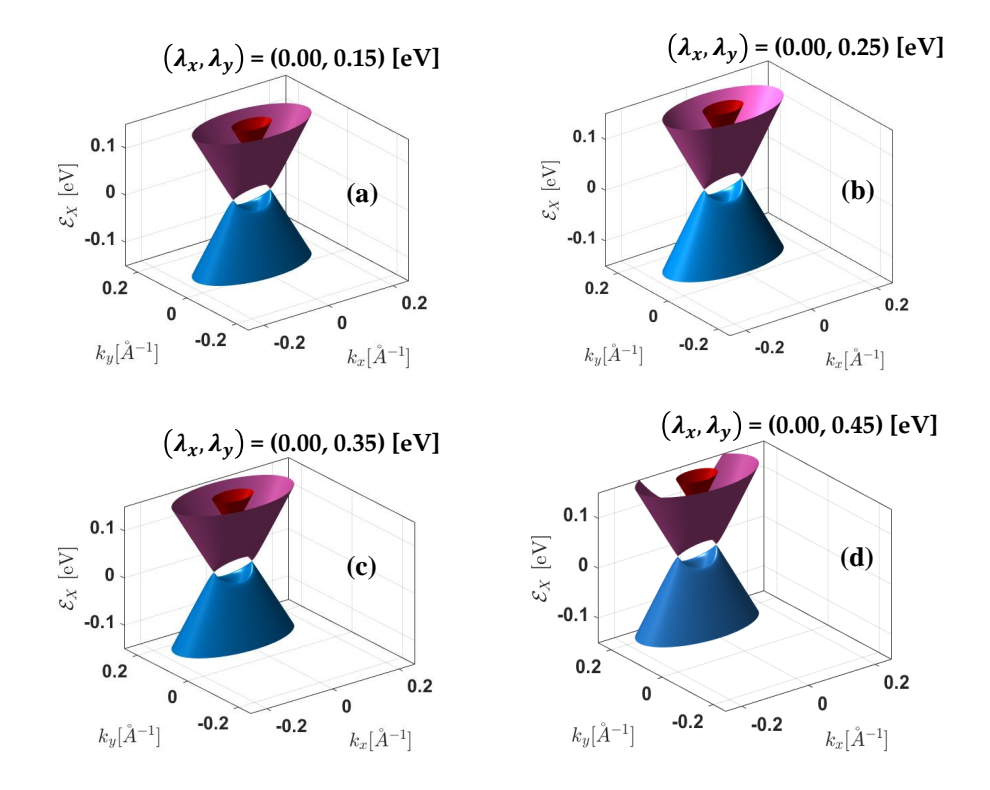


Fig. 6. The evolution of the three-dimensional energy band structure of Dirac fermions on the SnTe(001) surface near the X point, as the EPC strength along the y-direction is varied, shows a slow shift of the bands along the same direction. Here, n = 0.07 eV and $\delta = 0.026$ eV.

As an extension of this work, we now analyze the influence of the parameters n and δ . The physical meaning of these parameters has been discussed in Sec. 2. First, we consider the effect of n and δ in the absence of EPC (the pristine case). Fig. 7 shows the DOS when $(\lambda_x, \lambda_y) = (0,0)$ and δ is fixed at 26 meV for several different values of n. The results show that when n=0, vHSs do not appear, and the DOS resembles that of monolayer graphene in the low-energy limit. However, when $n \neq 0$, vHSs emerge, with their intensity increasing as n increases, although their positions remain independent of n. Moreover, the system remains in a semimetallic phase for all values of n. Next, we examine the variation of the DOS with respect to the parameter δ . In Fig. 8, we plot the DOS for a fixed value of n = 0.07 eV at several different values of δ . It can be seen that when $\delta = 0$, vHSs do not appear and the system is metallic, as indicated by the black curve. However, when $\delta \neq 0$, vHSs emerge, and the system consistently remains in a semimetallic phase. Interestingly, although δ varies, the vHSs always appear at energy values equal to δ . From Figs. 7 and 8, it can be concluded that the appearance of van Hove singularities requires both parameters n and δ to be nonzero. Additionally, the energy values at which the vHSs occur depend solely on δ and are independent of n. Finally, we examine the influence of the parameters n and δ on the DOS in the presence of EPC. Figs. 9 and 10 show the DOS for the same values of n and δ as considered in Figs. 7 and 8, respectively, but now we include EPC with $\lambda_x = \lambda_v = 0.45$ eV. It can be observed that when EPC is present with sufficiently strong intensity – as considered in Fig. 3

– the van Hove singularities do not appear for any values of n and δ , and the system becomes a narrow-gap semiconductor. Notably, the band gap decreases as the value of either n or δ increases. For example, in Fig. 9 with $\delta = 0.026$ eV, increasing n from 0 to 0.105 eV causes the band gap to decrease by nearly a factor of four. Similarly, in Fig. 10 with n = 0.07 eV, increasing δ from 0 to 0.065 eV results in the band gap being reduced by approximately half.

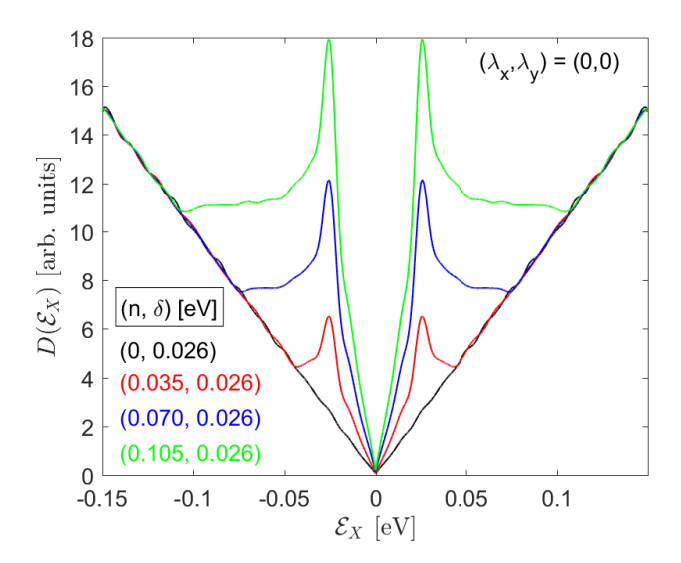


Fig. 7. The electronic DOS of the pristine SnTe(001) surface near the *X* point of SBZ for different values of parameter *n* at $\delta = 0.026$ eV.

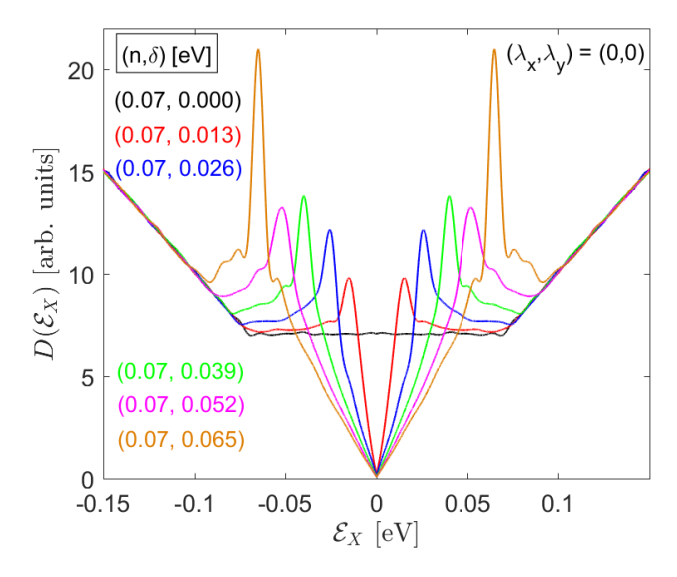


Fig. 8. The electronic DOS of the pristine SnTe(001) surface near the *X* point of SBZ for different values of parameter δ at n = 0.07 eV.

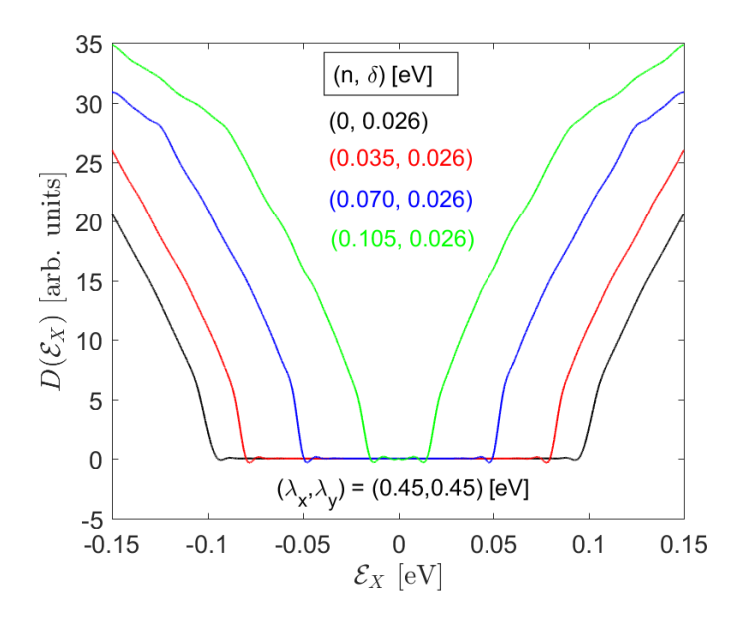


Fig. 9. The electronic DOS of the SnTe(001) surface near the X point of SBZ for different values of parameter n at $\delta=0.026$ eV. Here, the EPC is taken into account with $\lambda_x=\lambda_y=0.45$ eV.

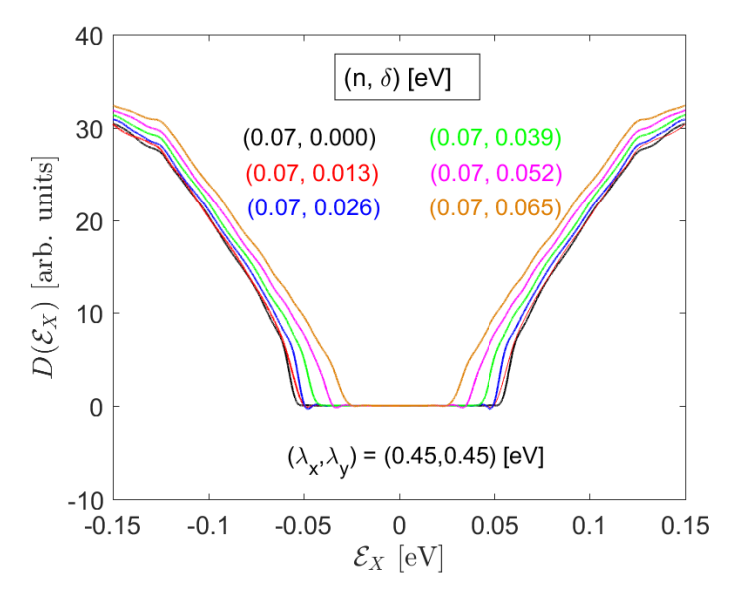


Fig. 10. The electronic DOS of the SnTe(001) surface near the *X* point of SBZ is shown for various values of the parameter δ , with n = 0.07 eV. The EPC strength used here is the same as in Fig. 9.

4. Conclusions

In this study, we investigated the effect of EPC on the vHS on the SnTe(001) surface, a TCI. Using a continuum Hamiltonian model and Green's function method, we calculated the electronic DOS and analyzed its dependence on parameters characterizing EPC. The EPC effect is incorporated through the momentum (wave number) components. When the EPC strength is varied along the x-direction, we observe a significant suppression of the vHS peaks. For sufficiently strong EPC, these singularities disappear entirely, and a band gap opens. In contrast, varying the EPC strength λ_v over a range comparable to λ_x produces only negligible changes in the DOS, and a strong EPC is needed to observe any small changes. This anisotropic response of the DOS to EPC strength highlights the inherent anisotropy of the SnTe(001) surface. Furthermore, we extended our study to examine the influence of intervalley scattering parameters, n and δ , on the system's electronic properties. These parameters also significantly affect the DOS, both in the absence and presence of EPC. Overall, our findings demonstrate that the electronic characteristics of the SnTe(001) surface can be effectively tuned via EPC – by altering lattice vibration-related factors such as temperature or substrate material – as well as through changes in intervalley scattering, which is governed by the surface roughness of the TCI. Experimentally, the energy band structure of pristine TCI surfaces, as well as its changes under the influence of physical factors, is expected to be observable using several modern techniques – for example, the angle-resolved photoemission spectroscopy (ARPES), as used in the earliest experimental studies on TCIs [6–8].

Acknowledgements

This research is funded by Vietnam National Foundation for Science and Technology Development (NAFOSTED) under grant number 103.01-2021.68.

Conflict of interest

The authors have no conflict of interest to declare.

References

- [1] M. Z. Hasan and C. L. Kane, Colloquium: Topological insulators, Rev. Mod. Phys. 82 (2010) 3045.
- [2] X.-L. Qi and S.-C. Zhang, Topological insulators and superconductors, Rev. Mod. Phys. 83 (2011) 1057.
- [3] L. Fu, Topological crystalline insulators, Phys. Rev. Lett. 106 (2011) 106802.
- [4] J. C. Y. Teo, L. Fu and C. L. Kane, Surface states and topological invariants in three-dimensional topological insulators: Application to Bi_{1-x}Sb_x, Phys. Rev. B **78** (2008) 045426.
- [5] T. H. Hsieh, H. Lin, J. Liu, W. Duan, A. Bansil and L. Fu, *Topological crystalline insulators in the SnTe material class*, Nat. Commun. 3 (2012) 982.
- [6] Y. Tanaka, Z. Ren, T. Sato, K. Nakayama, S. Souma, T. Takahashi et al., Experimental realization of a topological crystalline insulator in SnTe, Nat. Phys. 8 (2012) 800.
- [7] P. Dziawa, B. J. Kowalski, K. Dybko, R. Buczko, A. Szczerbakow, M. Szot et al., Topological crystalline insulator states in $Pb_{1-x}Sn_xSe$, Nat. Mater. 11 (2012) 1023.
- [8] S.-Y. Xu, C. Liu, N. Alidoust, M. Neupane, D. Qian, I. Belopolski *et al.*, Observation of a topological crystalline insulator phase and topological phase transition in $Pb_{1-x}Sn_xTe$, Nat. Commun. **3** (2012) 1192.
- [9] J. Wang, N. Wang, H. Huang and W. Duan, Electronic properties of snte-class topological crystalline insulator materials*, Chin. Phys. B 25 (2016) 117313.
- [10] H. Zhang, C.-X. Liu, X.-L. Qi, X. Dai, Z. Fang and S.-C. Zhang, Topological insulators in Bi₂Se₃, Bi₂Te₃ and Sb₂Te₃ with a single Dirac cone on the surface, Nat. Phys. **5** (2009) 438.

- [11] J. E. Moore and L. Balents, *Topological invariants of time-reversal-invariant band structures*, Phys. Rev. B **75** (2007) 121306.
- [12] A. P. Schnyder, S. Ryu, A. Furusaki and A. W. W. Ludwig, Classification of topological insulators and superconductors in three spatial dimensions, Phys. Rev. B 78 (2008) 195125.
- [13] R. Roy, Topological phases and the quantum spin Hall effect in three dimensions, Phys. Rev. B 79 (2009) 195322.
- [14] M. Kargarian and G. A. Fiete, Topological crystalline insulators in transition metal oxides, Phys. Rev. Lett. 110 (2013) 156403.
- [15] T. H. Hsieh, J. Liu and L. Fu, Topological crystalline insulators and dirac octets in antiperovskites, Phys. Rev. B 90 (2014) 081112.
- [16] C.-X. Liu, R.-X. Zhang and B. K. VanLeeuwen, Topological nonsymmorphic crystalline insulators, Phys. Rev. B 90 (2014) 085304.
- [17] W. Wu, Z. Shi, M. Ozerov, Y. Du, Y. Wang, X.-S. Ni et al., The discovery of three-dimensional van hove singularity, Nat. Commun. 15 (2024) 2313.
- [18] I. H. F. L. Yuan, Noah F. Q., Magic of high-order van hove singularity, Nat. Commun. 10 (2019) 5769.
- [19] L. Van Hove, *The occurrence of singularities in the elastic frequency distribution of a crystal*, Phys. Rev. **89** (1953) 1189.
- [20] R. S. Markiewicz, *The Van Hove Singularity and High-Tc Superconductivity: The Role of (Nanoscopic) Disorder*, pp. 555–560. Springer US, Boston, MA, 1991.
- [21] Y. Yang, G. Fedorov, S. E. Shafranjuk, T. M. Klapwijk, B. K. Cooper, R. M. Lewis et al., Electronic transport and possible superconductivity at van hove singularities in carbon nanotubes, Nano Lett. 15 (2015) 7859.
- [22] X. Chen, L. Wang, J. Ishizuka, R. Zhang, K. Nogaki, Y. Cheng et al., Coexistence of near-E_F flat band and van hove singularity in a two-phase superconductor, Phys. Rev. X 14 (2024) 021048.
- [23] K. X. Wang, Y. Guo and Z. Yu, Chapter three light trapping in photonic structures, in Photonic Crystal Metasur-face Optoelectronics, W. Zhou and S. Fan, eds., vol. 100 of Semiconductors and Semimetals, pp. 45–91, Elsevier, (2019), DOI.
- [24] T. Cea, N. R. Walet and F. Guinea, Electronic band structure and pinning of fermi energy to van hove singularities in twisted bilayer graphene: A self-consistent approach, Phys. Rev. B 100 (2019) 205113.
- [25] R. W. Havener, Y. Liang, L. Brown, L. Yang and J. Park, Van hove singularities and excitonic effects in the optical conductivity of twisted bilayer graphene, Nano Lett. 14 (2014) 3353.
- [26] P. Knüppel, J. Zhu, Y. Xia, Z. Xia, Z. Han, Y. Zeng et al., Correlated states controlled by a tunable van hove singularity in moire wse2 bilayers, Nat. Commun. 16 (2025) 1959.
- [27] H. Wang, H. Yuan, S. Sae Hong, Y. Li and Y. Cui, *Physical and chemical tuning of two-dimensional transition metal dichalcogenides*, Chem. Soc. Rev. 44 (2015) 2664.
- [28] G. G. Naumis, S. Barraza-Lopez, M. Oliva-Leyva and H. Terrones, *Electronic and optical properties of strained graphene and other strained 2d materials: a review*, Rep. Prog. Phys. **80** (2017) 096501.
- [29] X. Chen, Z. Zhou, B. Deng, Z. Wu, F. Xia, Y. Cao et al., Electrically tunable physical properties of twodimensional materials, Nano Today 27 (2019) 99.
- [30] M. Yarmohammadi and H. Cheraghchi, Effective low-energy RKKY interaction in doped topological crystalline insulators, Phys. Rev. B 102 (2020) 075411.
- [31] M. Yarmohammadi and K. Mirabbaszadeh, Enhancement of the anisotropic thermoelectric power factor of topological crystalline insulator snte and related alloys via external perturbations, J. Mater. Chem. A 7 (2019) 25573.
- [32] M. Yarmohammadi, S. R. Koshkaki, J. Berakdar, M. Bukov and M. H. Kolodrubetz, Probing topological phases in a perturbed kane-mele model via rkky interaction: Application to monolayer jacutingaite pt₂hgse₃, Phys. Rev. B 111 (2025) 014440.
- [33] M. Yarmohammadi, M. Bukov and M. H. Kolodrubetz, Noncollinear twisted RKKY interaction on the optically driven SnTe(001) surface, Phys. Rev. B 107 (2023) 054439.
- [34] J. Liu, W. Duan and L. Fu, Two types of surface states in topological crystalline insulators, Phys. Rev. B 88 (2013) 241303.
- [35] M. Ezawa, Valleytronics on the surface of a topological crystalline insulator: Elliptic dichroism and valley-selective optical pumping, Phys. Rev. B 89 (2014) 195413.
- [36] M. Serbyn and L. Fu, *Symmetry breaking and landau quantization in topological crystalline insulators*, Phys. Rev. B **90** (2014) 035402.

- [37] H. Cheraghchi and M. Yarmohammadi, Anisotropic ferroelectric distortion effects on the RKKY interaction in topological crystalline insulators, Scientific Reports 11 (2021) 5273.
- [38] Y. Okada, M. Serbyn, H. Lin, D. Walkup, W. Zhou, C. Dhital et al., Observation of Dirac node formation and mass acquisition in a topological crystalline insulator, Science 341 (2013) 1496.
- [39] K. D. Pham, N. T. Binh, H. Viet, N. T. Dung and B. D. Hoi, Controlling anisotropic surface group velocity and effective mass in topological crystalline insulator snte by rashba effect, Physica E: Low-dimensional Systems and Nanostructures 120 (2020) 114118.
- [40] D. Walkup, B. A. Assaf, K. L. Scipioni, R. Sankar, F. Chou, G. Chang et al., Interplay of orbital effects and nanoscale strain in topological crystalline insulators, Nat. Commun. 9 (2018) 1550.
- [41] C. Fang, M. J. Gilbert and B. A. Bernevig, *New class of topological superconductors protected by magnetic group symmetries*, Phys. Rev. Lett. **112** (2014) 106401.
- [42] Y. Okada, M. Serbyn, H. Lin, D. Walkup, W. Zhou, C. Dhital et al., Observation of dirac node formation and mass acquisition in a topological crystalline insulator, Science 341 (2013) 1496.
- [43] T. Yokoyama, Spin and valley transports in junctions of dirac fermions, New Journal of Physics 16 (2014) 085005.
- [44] G. Mahan, Many-Particle Physics, Physics of Solids and Liquids. Springer, 2000.